catalysts

MDPI

Article

Mechanochemical Synthesis of Nickel-Modified Metal–Organic Frameworks for Reduction Reactions

Paulette Gómez-López [1], Martyna Murat [2], José M. Hidalgo-Herrador [2], Carolina Carrillo-Carrión [1], Alina M. Balu [1], Rafael Luque [1,*] and Daily Rodríguez-Padrón [1,*]

[1] Departamento de Química Orgánica, Campus de Rabanales, Universidad de Córdoba, Edificio Marie Curie (C-3), Ctra Nnal IV-A, Km 396, E14014 Cordoba, Spain; gomezl.paulette@gmail.com (P.G.-L.); carrillocarrion.carolina@gmail.com (C.C.-C.); qo2balua@uco.es (A.M.B.)

[2] Research Department, ORLEN UniCRE a.s., Revoluční 1521/84, 400 01 Ústí nad Labem, Czech Republic; martyna.murat@gmail.com (M.M.); jose.hidalgo@unicre.cz (J.M.H.-H.)

* Correspondence: q62alsor@uco.es (R.L.); dailydggs@gmail.com (D.R.-P.)

Abstract: In this work, we report the incorporation of nickel oxide nanoparticles into a metal–organic framework (MOF) structure by a solvent-free mechanochemical strategy. In particular, the zirconium-based MOF UiO-66 was modified with different Ni loadings and characterized using complementary techniques including X-ray diffraction (XRD), N_2 porosimetry and X-ray photoelectron spectroscopy (XPS). The catalytic potential of the as-prepared Ni/UiO-66 materials in the hydrogenation reaction of methyl levulinate using 2-propanol as hydrogen donor solvent has been investigated under flow conditions. Under optimized conditions, the 5%Ni/UiO-66 led to the best catalytic performance (70% yield, 100% selectivity to gamma-valerolactone), which could be attributed to the higher content of the Ni species within the MOF structure. The obtained results are promising and contribute to highlighting the great potential of MOFs in biomass upgrading processes, opening the path to the sustainable development of the chemical industry.

Keywords: metal–organic frameworks; zirconium-based catalysts; biomass valorization; methyl levulinate hydrogenation

Citation: Gómez-López, P.; Murat, M.; Hidalgo-Herrador, J.M.; Carrillo-Carrión, C.; Balu, A.M.; Luque, R.; Rodríguez-Padrón, D. Mechanochemical Synthesis of Nickel-Modified Metal–Organic Frameworks for Reduction Reactions. *Catalysts* **2021**, *11*, 526. https://doi.org/10.3390/catal11050526

Academic Editors: Rubén Mas Ballesté and José Alemán

Received: 22 March 2021
Accepted: 13 April 2021
Published: 21 April 2021

1. Introduction

Population growth, spreading industrialization, and improving living standards, alongwith the associated per-capita consumption, are diminishing natural resources, particularly non-renewable fossil-derived reserves. Under this situation, one of the main challenges in the 21st century is to reduce our dependence on fossil fuels by developing more efficient and sustainable methodologies to produce chemicals, biofuels and other materials [1]. A key factor for achieving sustainable development, as included in the 2030 Agenda of the United Nations, is the valorization of waste raw materials. In this direction, lignocellulosic biomass has been proposed to be an effective renewable carbon-neutral resource, and importantly, is globally available [2,3].

Countless catalytic strategies have been developed for the conversion of lignocellulosic biomass into a wide range of chemicals. In this regard, levulinic acid (LA) is listed in the top 12 sugar-derived building blocks [4] that can serve as feedstocks for the production of other value-added chemicals or liquid fuels [5]. Among the chemicals obtained from LA or their alkyl levulinates derivates, gamma-valerolactone (GVL) has drawn considerable attention owing to its unique features (i.e., it is a biodegradable and nontoxic compound), and its broad range of applications (e.g., as an efficient fuel additive, a safe food additive, a green solvent, or as a raw material for organic synthesis) [2]. Numerous metal-based heterogeneous catalysts have been used for GVL production [6,7], suggesting that there are two key aspects of the catalytic system for achieving efficient and selective conversions. On the one hand, high metal dispersion within the support, and good metal accessibility, are

crucial. On the other hand, the transformation of LA or its alkyl derivates to GVL involves a series of alternately acid-catalyzed and metal-catalyzed processes, and thus bifunctional catalysts are required for a better catalytic performance [8]. Keeping these requirements in mind, metal–organic frameworks (MOFs) are novel porous materials based on inorganic metals and multidentate organic ligands, which can not only act as catalytic materials themselves but also serve as support for diverse catalytic units (e.g., metal and metal oxide nanoparticles, organic functional groups). The unique structural features of MOFs promote the metal dispersion and avoid metal leaching, and they can be easily modified with additional functionalities, thereby leading to outstanding catalytic performance in a myriad of different chemical transformations [9–11], including, for example, the production of GVL [12–14]. In this regard, our group has reported the use of a zirconium-based MOF, UiO-66, to carry out the transformation of methyl levulinate (ML) to GVL via catalytic transfer hydrogenation (CTH) under continuous flow [12]. Importantly, the amphoteric properties of the UiO-66 MOF play a key role in the aforementioned processes. In particular, it was found that Zr^{4+}–O^{2-} acid–base pair sites located in the Zr–oxo clusters were responsible for favoring the catalytic transfer hydrogenation of ML. Moreover, the Brönsted acidity of the μ_3-OH groups and organic linker defect sites could also benefit the cyclization step in the GVL production [15,16]. Although UiO-66 MOFs presented superior catalytic performance in the production of GVL (83% yield, 89% selectivity, 92.3 $mmol \cdot g^{-1} \cdot h^{-1}$ GVL productivity) as compared to reported Zr-based catalysts [12], it may be possible to enhance the catalytic activity of these MOFs by doping the material with another transition metal. Several studies have presented the use of Ru, Pt, Ir and Pd for hydrogenation reactions, due to their catalytic activity and efficiency. Nonetheless, such metals are highly expensive, whereas Ni is, comparatively, 100-fold cheaper. Ni nanoparticles possess a series of unusual properties and exhibit an excellent catalytic activity [17]. Moreover, Ni-based compounds have presented outstanding catalytic results for several organic reactions, such as hydrogenation and allylic akylation reactions [18–20].

Motivated by the aforementioned premises, and due to the experience of our group in mechanochemistry, as a green (no solvents required) and effective (high loading efficiency) synthetic approach for the incorporation of metals into porous supports (e.g., SBA-15, MCM-41, MOFs), [21,22], we herein propose the mechanochemical incorporation of Ni entities in the surface of UiO-66 MOFs and their further application for the production of GVL. It is worth noting that the conversion of ML into GVL is carried out using isopropanol as a hydrogen donor (no requirement for high-pressure molecular H_2) and under flow conditions, which is an alternative from an industrial point of view.

2. Results and Discussion

Mechanochemistry emerged as one of the most sustainable techniques for the preparation of nanomaterials, including metal and metal oxide nanoparticles, functionalized mesoporous materials, perovskites and bioconjugates. This work takes benefit of mechanochemistry for the post-synthesis modification of MOFs, particularly for the incorporation of Ni species within the structure of UiO-66, demonstrating good suitability, attending to the performed full-characterization, as detailed below.

N_2 adsorption–desorption measurements of all samples were performed to obtain insights into their textural properties. N_2 physisorption analysis of UiO-66 displayed certain microporosity, as suggested from the obtained isotherm (type 1), showing a sharp increase at $P/P_0 < 0.1$ (Figure 1A). UiO-66 sample exhibited an outstanding surface area of 1399 $m^2 \cdot g^{-1}$. Mechanochemical incorporation of nickel entities considerably affects the textural properties of the samples. As can be observed in Figure 1B–D, N_2 adsorption–desorption isotherms were shown to be type IV, which is typical of mesoporous materials. The observed modification could be ascribed to the collapse of UiO-66 architecture due to the mechanochemical treatment, while Ni content seems not to have a critical influence on the surface area of the samples, displaying values of 496, 465 and 444 $m^2 \cdot g^{-1}$ for 1%Ni/UiO-66, 3%Ni/UiO-66 and 5%Ni/UiO-66, respectively.

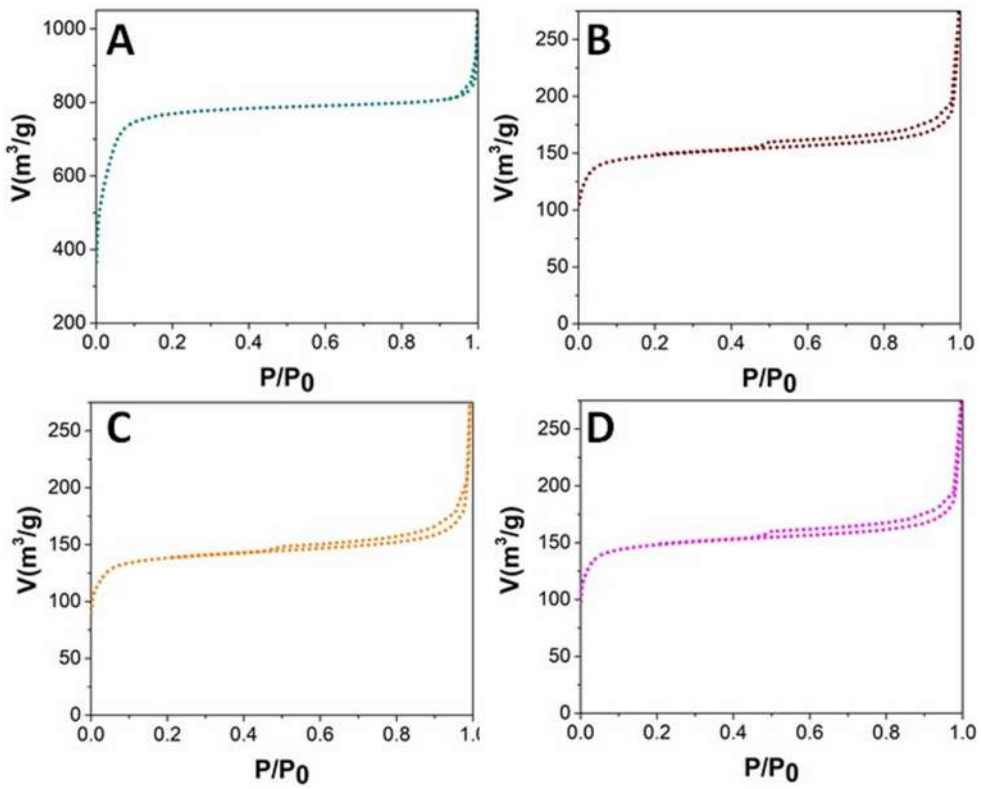

Figure 1. N_2 adsorption–desorption isotherms of (**A**) UiO-66, (**B**) 1%Ni/UiO-66, (**C**) 3%Ni/UiO-66, (**D**) 5%Ni/UiO-66.

The crystal structure and arrangement of the materials was investigated by XRD analysis; as shown in Figure 2A, XRD patterns of all samples displayed the presence of two main peaks located at 7.5° and 8.6°, which are associated with (111) and (002) crystallographic planes, respectively, and are typically observed in UiO-66 MOFs reported in the literature [23,24]. Such results confirmed both the successful synthesis of UiO-66 MOFs and the suitability of the mechanochemical approach for the modification of MOFs with metal entities. Even if the presence of both peaks related to the main crystallographic planes of UiO-66 indicated the retention of the crystal structure, certain amorphization occurred after the incorporation of higher Ni amounts in the sample [25,26]. Magnified XRD diffractograms (Figure 2B–E) revealed the typical characteristic pattern UiO-66 but with a clear decrease in crystallinity in the samples with 3 and 5% Ni. No clear evidence of the presence of Ni were found by XRD analysis, as was expected due to the low Ni percentages in the samples.

In order to study the electronic properties of the samples and to corroborate the incorporation of Ni entities on the UiO-66 surface, XPS analysis was carried out (Figure 3). XPS results revealed the presence of carbon, oxygen, zirconium and nickel, as suggested from the acquired regions. In particular, the C1s and O1s XPS regions exhibited certain modifications after the mechanochemical incorporation of Ni. The C1s region of the UiO-66 sample displayed the presence of three main contributions around 284.0, 285.1 and 287.9 eV, related to C−C/C=C, C=O and COO, respectively (Figure 3A). Samples modified with Ni showed lower contributions of C=O and COO^- signals, most likely due to interactions between the oxygen groups and the Ni entities during the mechanochemical treatment [27]. Similar behavior was observed in the O1s region after Ni incorporation (Figure 3B). The O1s XPS region of UiO-66 material displayed the presence of two main signals located at 531.9 and 533.5 eV, attributed to O-Zr and Zr-O-C bonds [28]. The observed increase in the peak at around 531.0 eV could be most likely attributed to the appearance and overlapping of a new signal related to the Ni-O bond, which has been reported in the literature to be around 529.9 eV for Ni^{2+} species [29]. Furthermore, the Zr 3d XPS region of

the four samples was acquired, as can be observed in Figure 3C. In all cases, Zr $3d_{5/2}$ peaks were located at ca. 182.4 eV, while the distance between Zr $3d_{5/2}$ y Zr $3d_{3/2}$ bands were shown to be ca. 2.5 eV, indicating the formation of Zr (IV) species [30]. Additionally, Ni XPS region was acquired for the three Ni modified samples. Due to the low percentage of Ni in the samples, Ni2p XPS signal was practically undetectable for 1%Ni/UiO-66, but, in any case, a clear increase in the band intensity could be observed for higher Ni content. Such a band seems to be located over 855.0 eV, which is related to Ni^{2+} species and demonstrated the successful incorporation of Ni entities on the UiO-66 surface [31,32]. Furthermore, a sample containing 10% of nickel has been prepared and characterized by XPS, as shown in Figure S1, where Ni2p XPS signal could be clearly visualized, displaying a higher intensity in accordance with the higher nickel content.

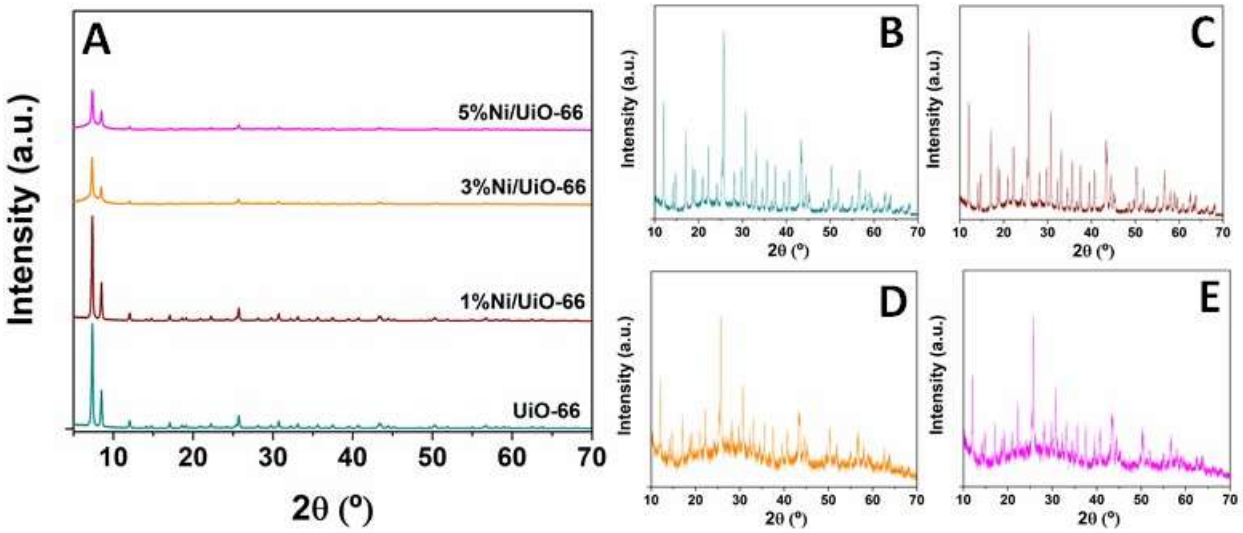

Figure 2. XRD patterns of the synthesized materials. (**A**) XRD diffractograms of all samples from 5° to 70°. Magnified XRD patterns from 10° to 70° for (**B**) UiO-66, (**C**) 1%Ni/UiO-66, (**D**) 3%Ni/UiO-66, (**E**) 5%Ni/ UiO-66.

Biomass valorization reactions could have a tremendous impact on the chemical industry for the replacement of petro-based feestocks [33,34]. Therefore, the catalytic behavior of the obtained samples was investigated in the continuous-flow transfer hydrogenation reaction of ML to GVL. Blank experiments were performed to confirm the role of the employed catalytic systems. No significant conversion of ML was obtained when the reaction was performed in the absence of catalyst. In turn, by carrying out the reaction using UiO-66, a conversion of 68% was obtained, with selectivity values towards GVL and isopropyl levulinate of 60% and 40%, respectively. A GVL yield of 40% was reached by employing UiO-66. Significantly, the herein investigated samples could be separated into: (a) unmodified UiO-66 sample and (b) mechanochemically modified UiO-66-derived samples, as shown in Figure 4. As previously commented, the employed mechanochemical strategy led to a drastic modification of the textural properties, which further influenced the catalytic response, resulting in a clear decrease in methyl levulinate conversion (22%), and consequently, a lower yield of GVL (12%) for the mechanochemically treated UiO-66 material. Nonetheless, nickel incorporation by mechanochemistry boosted the catalytic activity in terms of conversion and yield, but more importantly, tuned the selectivity towards GVL, with values higher than 99% for the three nickel modified samples, which could further facilitate purification steps. Conversion values for 1%Ni/UiO-66 and 3%Ni/UiO-66 samples were found to be 30% and 48%, respectively, while the conversion increased to 69% for 5%Ni/UiO-66, retaining the excellent GVL selectivity. Such results demonstrated the clear influence of nickel content on the catalytic behavior of the samples, compensating the negative influence that the mechanochemical process itself could have on the textural features of the materials. In addition, mechanochemistry has evident advantages in com-

parison with other techniques for incorporation of nanoparticles, due to its high simplicity and environmentally friendly character, also validating the proposed methodology.

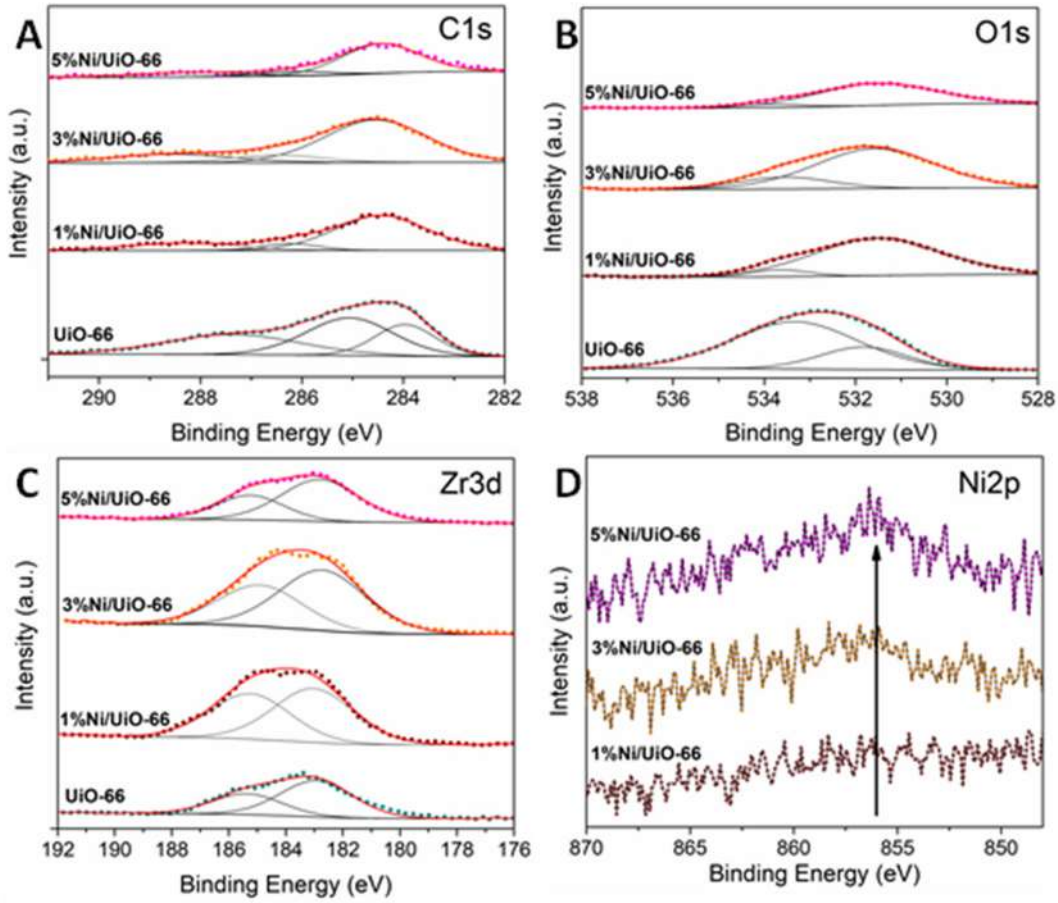

Figure 3. XPS spectra of the prepared samples in the (**A**) C1s, (**B**) O1s, (**C**) Zr3d and (**D**) Ni2p regions.

In order to investigate the influence of higher nickel content in the materials, a sample containing 10% of nickel was prepared and tested in the studied reaction (Figure S2). By employing such sample, conversion values of 73% were reached. However, it should be noted that conversion values of around 70% are already obtained by employing the 5%Ni/UiO-66 catalytic system and, in addition, special attention should be devoted to the cost-efficiency of the processes; thus a lower concentration of metal is desired.

The stability of the samples was investigated along 180 min of run time, as displayed in Figure 5. UiO-66 and 1%Ni/UiO-66 samples achieved a pseudo-stationary state after 100 min of reaction, while for 3%Ni/UiO-66 and 5%Ni/UiO-66 materials, the pseudo-stationary state was reached after 120 min. In particular, 5%Ni/UiO-66, exhibiting the most promising results, displayed an increase in the conversion along the first 100 min, most likely due to a thermal activation during the reaction and/or the pre-adsorption of methyl levulinate on the catalyst surface. Remarkably, no variation in the selectivity values were found for mechanochemically Ni-modified samples, confirming the good stability of the materials under continuous flow conditions.

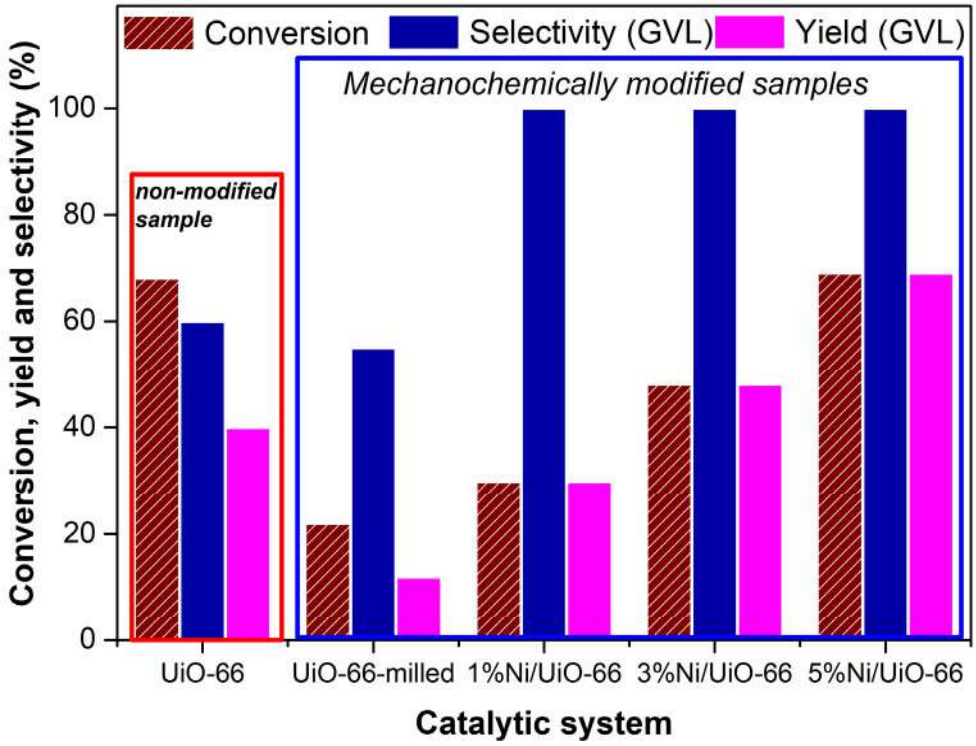

Figure 4. Comparative analysis of the catalytic performance in terms of conversion of methyl levulinate, selectivity and yield towards GVL of UiO-66, 1%Ni/UiO-66, 3%Ni/UiO-66, 5%Ni/UiO-66.

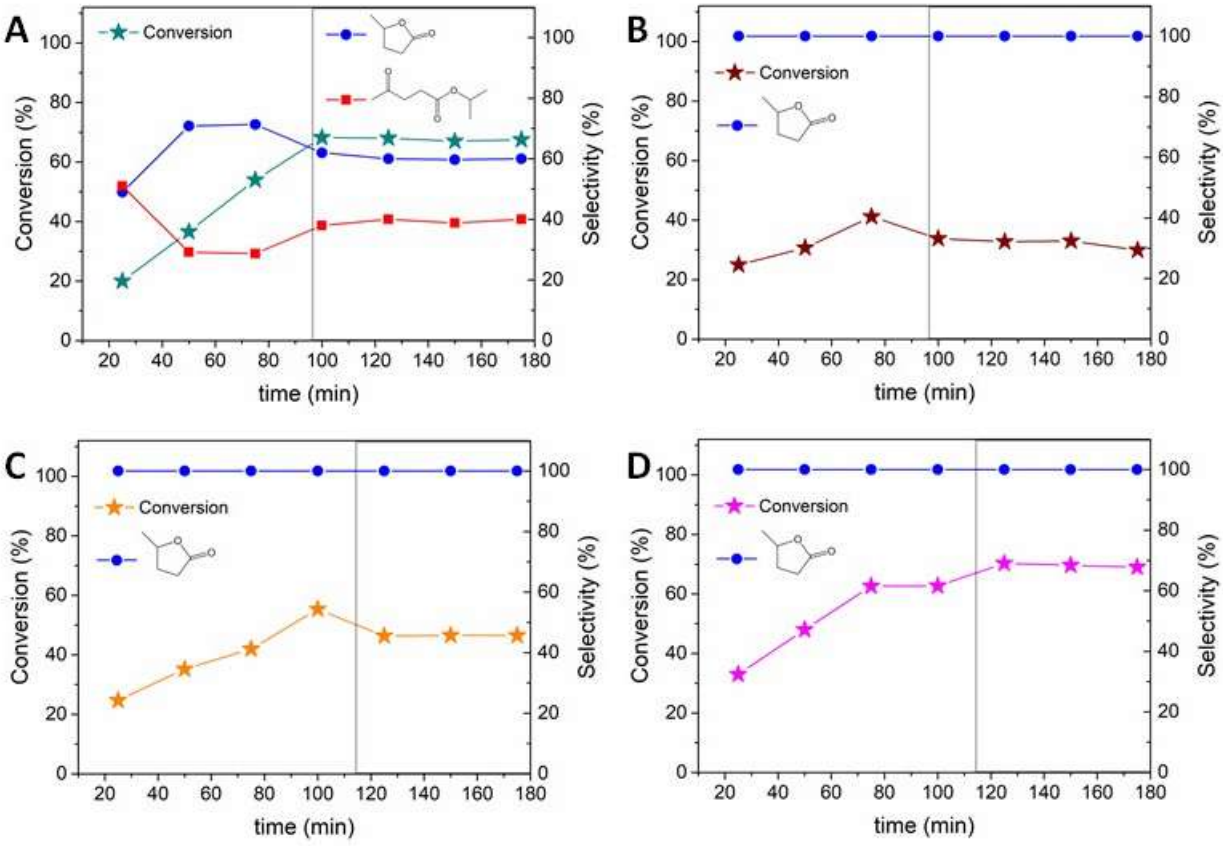

Figure 5. Catalytic performance in terms of stability, along run times of 180 min for (**A**) UiO-66, (**B**) 1%Ni/UiO-66, (**C**) 3%Ni/UiO-66, (**D**) 5%Ni/UiO-66.

3. Experimental

3.1. Preparation of Ni/UiO-66 MOFs

The synthesis of UiO-66 was carried out following a previously reported procedure [12]. In this typical procedure, a mixture of zirconium (IV) chloride ($ZrCl_4$) (2 g, 8.54 mmol) and 16 mL hydrochloric acid (37%) was first added to 80 mL to dimethylformamide (DMF) and sonicated for 20 min. Thereafter, therephthalic acid (2 g, 12 mmol) previously dissolved in 80 mL DMF were added to the above mixture and sonicated for another 20 min. The mixture was then transferred to a 500 mL teflon bottle and heated at 120 °C for 24 h in an oven. The generated precipitate was separated by filtration, washed first with DMF (100 mL × 2 × 30 min) and then with methanol (100 mL × 2 × 30 min), and finally dried and activated at 80 °C under vacuum.

In the second step, Ni was incorporated within the UiO-66 by a mechanochemical protocol, employing $Ni(NO_3)_2{\cdot}6H_2O$. Samples containing different Ni percentages, namely 1, 3, 5 and 10%, were prepared by mixing 1 g of UiO-66 with 50 mg, 148 mg, 248 mg and 496 mg of nickel (II) nitrate hexahydrate, respectively, in a Retsch (Haan, Germany) PM100 ball mill. The preparation of the materials was carried out by milling at 350 rpm during 10 min (with reverse rotation and interval times of 5 s), employing a 125 mL reaction chamber and eighteen 10 mm stainless balls. The obtained samples were recovered from the reaction chamber and finally thermally treated at 200 °C for 2 h, obtaining 1%, 3% 5% and 10%Ni/UiO-66 materials.

3.2. Catalysts Characterization

XRD diffractograms of the materials prepared in this work were acquired in a Bruker model DISCOVER D8 diffractogram (Billerica, MA, USA), and recorded in a 2θ scan range from 3° to 70°. Bruker Diffrac. suite plus Eva software (3), supported by Power Diffraction File database, was used for phase identification. The textural properties of the materials were evaluated by N_2 adsorption/desorption measurements using a Micromeritics Accelerated Surface Area and Porosimetry (ASAP) 2000. The materials were degassed at 130 °C for 24 h (p < 0.1 Pa) prior to analysis. XPS experiments were performed in a SpecsTM ultrahigh vacuum (UHV) multipurpose surface analysis system, equipped with the Phoibos 150-MCD (Multi Channeltron Detector) energy detector (Berlin, Germany). The measurements were carried out at pressures $<10^{-10}$ mbar, employing an X-ray source in a "stop and go" mode. The XPS CASA program was used to analyze the obtained data.

3.3. Catalytic Experiments

In this work, the catalytic performance of the as-prepared Ni/UiO-66 materials was evaluated in the transfer hydrogenation reaction of methyl levulinate (ML) to gamma-valerolactone (GVL) using a Phoenix continuous-flow reactor (Budapest, Hungary) and 2-propanol as hydrogen donor solvent [35]. The reaction conditions were, in accordance with previously explored reaction conditions [36], 200 °C and 30 bars of pressure. The catalysts (1%Ni/UiO-66, 3%Ni/UiO-66 or 5%Ni/UiO-66) were packed (0.2 g of catalyst per cartridge) in a 30 mm long ThalesNano CatCart. Firstly, a solution of ML (0.3 M, in 2-propanol) was passed through the catalyst bed at a flow rate of 0.2 mL/min. The samples were collected every 25 min for further analysis by GC-MS.

The collected samples were analyzed by gas chromatography-flame-ionization detector (GC-FID, Agilent 5890 Series II, Waltham, MA, USA) equipped with a FID detector and SUPELCO EQUITY TM-1 fused silica capillary column (60 m × 0.25 mm × 0.25μm). The injector and detector temperatures were set as 250 °C. The GC oven program was the following: 60 °C (1 min) to 230 °C at 10 °C/min (hold 5 min) for a total run time of 23 min. In addition, the collected aliquots were analyzed by gas chromatography-mass spectrometer (GC-MS, Agilent 5977B Series GC/MSD System, Waltham, MA, USA) in order to identify the obtained products.

Conversion and selectivity were calculated from the GC-FID data by using these Equations:

$$Conversion\ (\%) = \frac{(C_{ML\ initial} - C_{ML\ final})}{C_{ML\ initial}} \times 100 \quad (1)$$

$$Selectivity\ (\%) = \frac{C_{GVL}}{\left[C_{ML\ initial} - C_{ML\ final}\right]} \times 100 \quad (2)$$

where $C_{ML\ initial}$ and $C_{ML\ final}$ are the concentrations of the *ML* before and after the reaction, respectively, and the C_{GVL} is the concentration of the product (*GVL*).

4. Conclusions

Mechanochemical modification of UiO-66 with nickel oxide nanoparticles was herein investigated. Besides its inherent advantages related to its simplicity, versatility, reproducibility and sustainable character, mechanochemical processes were shown to be effective for the incorporation of metal oxide entities on the surface of the aforementioned metal–organic framework, as confirmed by XPS analysis. However, the mechanochemical strategy also resulted in a 65% decrease in the initial surface area. Such behavior was expected according to previous investigations on the effect of mechanochemical approaches on the textural properties of materials. In any case, the samples retained a feasible surface area, over 400 m^2/g, and, more importantly, the nickel modified samples exhibited a greatly improved selectivity towards GVL—higher than 99%—and a maximum conversion value of 69%.

Supplementary Materials: The following are available online at https://www.mdpi.com/article/10.3390/catal11050526/s1, Figure S1: Ni 2p XPS spectra of the nickel modified samples, including the 10%Ni/UiO-66 material; Figure S2: Comparative analysis of the catalytic performance in terms of conversion of methyl levulinate, selectivity and yield towards GVL of 5%Ni/UiO-66 and 10%Ni/UiO-66.

Author Contributions: Conceptualization, R.L. and J.M.H.-H., methodology, D.R.-P. and R.L.; software, J.M.H.-H.; validation, A.M.B., D.R.-P. and R.L.; formal analysis, D.R.-P.; investigation, P.G.-L. and M.M.; resources, J.M.H.-H. and R.L.; data curation, D.R.-P., C.C.-C. and A.M.B.; writing—original draft preparation, P.G.-L., M.M.; writing—review and editing, D.R.-P., A.M.B. and R.L.; visualization, J.M.H.-H. and R.L.; supervision, A.M.B., J.M.H.-H. and R.L.; project administration, J.M.H.-H. and R.L.; funding acquisition, J.M.H.-H. and R.L. All authors have read and agreed to the published version of the manuscript.

Funding: This work has been supported by the Efficient Use of Energy Resources Using Catalytic Processes (LM20189) project, which has been financially supported by MEYS within the targeted support of large infrastructures. MINECO is gratefully acknowledged for funding project PID2019-109953GB-I00. Universidad de Cordoba (Spain) has also supported this work.

Acknowledgments: The publication is a result of the project which was carried out with the financial support of the Ministry of Industry and Trade of the Czech Republic, with institutional support for the long-term conceptual development of research organisation. The result was achieved using the infrastructure included in the Efficient Use of Energy Resources Using Catalytic Processes (LM20189) project, which has been financially supported by MEYS within the targeted support of large infrastructures. PG-L gratefully acknowledges the support of CONACYT-México for the international fellowship number 709621. C.C.-C., R.L. gratefully acknowledges the Ministerio de Ciencia e Innovacion, Gobierno de España as well as FEDER funds under project PID2019-109953GB-I00 and financial support from the Universidad de Cordoba (Spain).

Conflicts of Interest: There are no conflict to declare.

References

1. Xu, C.; Paone, E.; Rodríguez-Padrón, D.; Luque, R.; Mauriello, F. Recent catalytic routes for the preparation and the upgrading of biomass derived furfural and 5-hydroxymethylfurfural. *Chem. Soc. Rev.* **2020**, *49*, 4273–4306. [CrossRef]
2. Horváth, I.T.; Mehdi, H.; Fábos, V.; Boda, L.; Mika, L.T. γ-Valerolactone—A sustainable liquid for energy and carbon-based chemicals. *Green Chem.* **2008**, *10*, 238–242. [CrossRef]
3. Kang, S.; Fu, J.; Zhang, G. From lignocellulosic biomass to levulinic acid: A review on acid-catalyzed hydrolysis. *Renew. Sustain. Energy Rev.* **2018**, *94*, 340–362. [CrossRef]
4. Werpy, T.; Petersen, G. Top Value Added Chemicals from Biomass: Volume I Results of Screening for Potential Candidates from Sugars and Synthesis Gas. *NRLE Naracoorte Reg. Livest. Exch.* **2004**, *94*, 340–362.
5. Huang, Y.B.; Yang, T.; Lin, Y.T.; Zhu, Y.Z.; Li, L.C.; Pan, H. Facile and high-yield synthesis of methyl levulinate from cellulose. *Green Chem.* **2018**, *20*, 1323–1334. [CrossRef]
6. Wright, W.R.; Palkovits, R. Development of heterogeneous catalysts for the conversion of levulinic acid to γ-valerolactone. *ChemSusChem* **2012**, *5*, 1657–1667. [CrossRef] [PubMed]
7. Dutta, S.; Iris, K.M.; Tsang, D.C.; Ng, Y.H.; Ok, Y.S.; Sherwood, J.; Clark, J.H. Green synthesis of gamma-valerolactone (GVL) through hydrogenation of biomass-derived levulinic acid using non-noble metal catalysts: A critical review. *Chem. Eng. J.* **2019**, *372*, 992–1006. [CrossRef]
8. Yu, Z.; Lu, X.; Xiong, J.; Ji, N. Transformation of levulinic acid to valeric biofuels: A review on heterogeneous bifunctional catalytic systems. *ChemSusChem* **2019**, *17*, 3915–3930. [CrossRef]
9. Pascanu, V.; González Miera, G.; Inge, A.K.; Martín-Matute, B. Metal–organic frameworks as catalysts for organic synthesis: A critical perspective. *J. Am. Chem. Soc.* **2019**, *18*, 7223–7234. [CrossRef]
10. Xu, C.; Fang, R.; Luque, R.; Chen, L.; Li, Y. Functional metal–organic frameworks for catalytic applications. *Coord. Chem. Rev.* **2019**, *388*, 268–292. [CrossRef]
11. Yang, D.; Gates, B.C. Catalysis by Metal Organic Frameworks: Perspective and Suggestions for Future Research. *ACS Catal.* **2019**, *3*, 1779–1798. [CrossRef]
12. Ouyang, W.; Zhao, D.; Wang, Y.; Balu, A.M.; Len, C.; Luque, R. Continuous Flow Conversion of Biomass-Derived Methyl Levulinate into γ-Valerolactone Using Functional Metal Organic Frameworks. *ACS Sustain. Chem. Eng.* **2018**, *5*, 6746–6752. [CrossRef]
13. Feng, J.; Zhong, Y.; Xie, M.; Li, M.; Jiang, S. Using MOF-808 as a Promising Support to Immobilize Ru for Selective Hydrogenation of Levulinic Acid to γ-Valerolactone. *Catal. Lett.* **2020**, *151*, 86–94. [CrossRef]
14. Feng, J.; Li, M.; Zhong, Y.; Xu, Y.; Meng, X.; Zhao, Z.; Feng, C. Hydrogenation of levulinic acid to γ-valerolactone over Pd@ UiO-66-NH2 with high metal dispersion and excellent reusability. *Micropor. Mesopor. Mat.* **2020**, *294*, 109858. [CrossRef]
15. Cirujano, F.G.; Corma, A.; Llabres Xamena, F.X. Zirconium-containing metal organic frameworks as solid acid catalysts for the esterification of free fatty acids: Synthesis of biodiesel and other compounds of interest. *Catal. Today* **2015**, *257*, 213–220. [CrossRef]
16. Ling, S.; Slater, B. Dynamic acidity in defective UiO-66. *Chem. Sci.* **2016**, *7*, 4706–4712. [CrossRef] [PubMed]
17. Heiz, U.; Vanolli, F.; Sanchez, A.; Schneider, W.D. Catalytic Oxidation of Carbon Monoxide on Monodispersed Platinum Clusters: Each Atom Counts. *J. Am. Chem. Soc.* **1998**, *120*, 9668–9671. [CrossRef]
18. Wang, J.; Wang, P.; Wang, L.; Li, D.; Wang, K.; Wang, Y.; Zhu, H.; Yang, D.; Wang, R. Nickel-Mediated Asymmetric Allylic Alkylation between Nitroallylic Acetates and Acyl Imidazoles. *Org. Lett.* **2017**, *19*, 4826–4829. [CrossRef] [PubMed]
19. Ngamnithiporn, A.; Jette, C.I.; Bachman, S.; Virgil, S.C.; Stoltz, B.M. Nickel-catalyzed enantioselective allylic alkylation of lactones and lactams with unactivated allylic alcohol. *Chem. Sci.* **2018**, *9*, 2547–2551. [CrossRef]
20. Sha, S.-C.; Jiang, H.; Mao, J.; Bellomo, A.; Jeong, S.A.; Walsh, P.J. Nickel-Catalyzed Allylic Alkylation with Diarylmethane Pronucleophiles: Reaction Development and Mechanistic Insights. *Angew. Chem.* **2016**, *55*, 1070–1074. [CrossRef] [PubMed]
21. Marquez-Medina, M.D.; Mhadmhan, S.; Balu, A.M.; Romero, A.A.; Luque, R. Post-synthetic mechanochemical incorporation of Al-species into the framework of porous materials: Toward more sustainable redox chemistries. *ACS Sustain. Chem. Eng.* **2019**, *10*, 9537–9543. [CrossRef]
22. Xu, C.; De, S.; Balu, A.M.; Ojeda, M.; Luque, R. Mechanochemical synthesis of advanced nanomaterials for catalytic applications. *Chem. Commun.* **2015**, *31*, 6698–6713. [CrossRef]
23. Zhang, X.; Song, L.; Bi, F.; Zhang, D.; Wang, Y.; Cui, L. Catalytic oxidation of toluene using a facile synthesized Ag nanoparticle supported on UiO-66 derivative. *J. Coll. Int. Sci.* **2020**, *571*, 38–47. [CrossRef]
24. Kandiah, M.; Nilsen, M.H.; Usseglio, S.; Jakobsen, S.; Olsbye, U.; Tilset, M.; Larabi, C.; Quadrelli, E.A.; Bonino, F.; Lillerud, K.P. Synthesis and Stability of Tagged UiO-66 Zr-MOFs. *Chem. Mat.* **2010**, *24*, 6632–6640. [CrossRef]
25. Rungtaweevoranit, B.; Baek, J.; Araujo, J.R.; Archanjo, B.S.; Choi, K.M.; Yaghi, O.M.G.; Somorjai, A. Copper Nanocrystals Encapsulated in Zr-based Metal–Organic Frameworks for Highly Selective CO_2 Hydrogenation to Methanol. *Nano Lett.* **2016**, *12*, 7645–7649. [CrossRef] [PubMed]
26. Bambalaza, S.E.; Langmi, H.W.; Mokaya, R.; Musyoka, N.M.; Khotseng, L. Experimental demonstration of dynamic temperature-dependent behaviour of UiO-66 metal-organic-framework: Compaction of hydroxylated and deydroxylated forms of UiO-66 for high pressure hydrogen storage. *ACS Appl. Mater. Interfaces* **2020**, *22*, 24883–24894. [CrossRef] [PubMed]

27. Zhao, C. Enhanced strength in reduced graphene oxide/nickel composites prepared by molecular-level mixing for structural applications. *Appl. Phys. A* **2014**, *118*, 409–416. [CrossRef]
28. Chen, D.; Sun, H.; Wang, Y.; Quan, H.; Ruan, Z.; Ren, Z.; Luo, X. UiO-66 derived zirconia/porous carbon nanocomposites for efficient removal of carbamazepine and adsorption mechanism. *Appl. Surf. Sci.* **2019**, *507*, 145054. [CrossRef]
29. Oswald, S.; Brückner, W. XPS depth profile analysis of non-stoichiometric NiO films. *Surf. Interface Anal.* **2004**, *36*, 17–22. [CrossRef]
30. Martin-Perales, A.I.; Rodríguez-Padrón, D.; Garcia, A.; Len, C.; de Miguel, G.; Muñoz-Batista, J.M.; Luque, R. Photocatalytic production of vanillin over CeOx and ZrO2 modified biomass-templated titania. *Ind. Eng. Chem. Res.* **2020**, *59*, 17085–17093. [CrossRef]
31. Defilippi, C.; Rodríguez-Padrón, D.; Luque, R.; Giordano, C. Simplifying Levulinic Acid Conversion Towards a Sustainable Biomass Valorisation. *Green Chem.* **2020**, *22*, 2929–2934. [CrossRef]
32. Peck, M.A.; Langell, M.A. Comparison of Nanoscaled and Bulk NiO Structural and Environmental Characteristics by XRD, XAFS, and XPS. *Chem. Mater.* **2012**, *23*, 4483–4490. [CrossRef]
33. Gumina, B.; Mauriello, F.; Pietropaolo, R.; Galvagno, S.; Espro, C. Hydrogenolysis of sorbitol into valuable C3-C2 alcohols at low H_2 pressure promoted by the heterogeneous Pd/Fe_3O_4 catalyst. *Mol. Catal.* **2018**, *446*, 152–160. [CrossRef]
34. Paone, E.; Beneduci, A.; Corrente, G.A.; Malara, A.; Mauriello, F. Hydrogenolysis of aromatic ethers under lignin-first conditions. *Mol. Catal.* **2020**, *497*, 111228. [CrossRef]
35. Rodríguez-Padrón, D.; Puente-Santiago, A.R.; Balu, A.M.; Muñoz-Batista, M.J.; Luque, R. Continuous Flow Synthesis of High Valuable N-Heterocycles via Catalytic Conversion of Levulinic Acid. *Front. Chem.* **2019**, *7*, 103. [CrossRef]
36. Lázaro, N.; Franco, A.; Ouyang, W.; Balu, A.M.; Romero, A.A.; Luque, R.; Pineda, A. Continuous-Flow Hydrogenation of Methyl Levulinate Promoted by Zr-Based Mesoporous Materials. *Catalysts* **2019**, *2*, 142. [CrossRef]